 doi:10.20944/preprints202107.0476.v1

Article

Fault Ride Through Capability Analysis of Wind Turbine with Doubly Fed Induction Generator

Salem Molla Endale [1], Milkias Berhanu Tuka [2,*]

[1] Adama Science and Technology University; salem.mola@gmail.com
[2] Adama Science and Technology University; mil_ber2000@astu.edu.et
* Correspondence: mil_ber2000@astu.edu.et

Abstract: Variable speed wind turbine with partial-scale power converter commonly known as Doubly Fed Induction Generator (DFIG) has a stator winding directly coupled with grid and rotor winding connected to the grid via a fault-prone back to back power converters. Grid failures are well-known to constitute a threat to DFIG. In early times, when a fault occurred, these generators were required to disengage from the grid in order to protect the generator and power converters. However, due to the increased penetration of wind turbines into the power system, grid operators demanded that the wind turbines remain connected to the grid, as disconnecting them would further disrupt the grid. When a failure occurs at the grid terminal, it causes a spike in stator current, which leads to a rise in rotor current. This high stator and rotor currents triggers the DC-link voltage to rise and eventually cause harm to the converters. Thus, this paper work integrates crowbar protection with a Battery Energy Storage System (BESS) to improve FRT capability. Moreover, the proposed protection system is compared to the crowbar protection system to demonstrate the effectiveness of the proposed method in improving the performance of the machine. MATLAB-Simulink software is used for modeling and simulation. All system parameters are obtained from ADAMA-II Wind Farm.

Keywords: Battery Energy Storage System; Crowbar; Fault Ride Through Capability; Vector control; Wind turbine

1. Introduction

One of the attractive characteristics of the a Doubly Fed Induction Generator (DFIG) is that it can provide decoupled active and reactive control of the generator through a variety of control techniques [1]. In DFIG, the winding of the stator is attached directly to the grid while the rotor is connected to the grid by the back-to-back converter. The Rotor Side Convertor (RSC) is used to control both the active and the reactive power as well as the torque and speed of the generator. While the Grid Side Convertor (GSC) is used to preserve DC-link voltage and deliver reactive power to the grid when necessary. These bidirectional power converters allow power to flow from the grid to the machine and vice versa. Thus, the machine can operate as a generator as well as a motor in both sub-synchronous and super-synchronous modes of operation. However, only the generator mode at both speeds is of great interest in wind power generation. Moreover, the GSC can function as an inverter (when the rotor supplies active power to the grid) or a rectifier, (when the rotor absorbs active power from the grid), depending on the mode of operation [1-2].

The power converter of DFIG can tolerate just 25-30% of the generator capacity, rendering the DFIG Wind Turbine (WT) highly susceptible and vulnerable to grid disturbance. When a grid fault causes a voltage drop, an increase in rotor voltage is expected to compensate for the stator voltage and stabilize the rotor currents. Nevertheless, due to the limited voltage of the converter, when the required rotor voltage exceeds this limit, it is no longer possible to regulate the current. This indicates that a voltage drop will result in a high induced voltage and current in the rotor circuit. Furthermore, the strong current

Preprints (www.preprints.org) | NOT PEER-REVIEWED | Posted: 21 July 2021 doi:10.20944/preprints202107.0476.v1

triggers the DC-link voltage to increase [3]. For decades, if such faults existed, generators had to be removed immediately from the grid to protect the generator, power converters, and the dc-link capacitor. However, as wind turbines are gradually being integrated into transmission systems, grid transmission and distribution operators and wind turbine manufacturers have introduced regulations for connecting generators to the grid even during faults [3]. These current grid codes enable the generator to remain connected to the grid even though faults occur. The capability of WT to remain attached to the grid during voltage dips is referred to as low voltage ride through (LVRT) and the key purpose of these requirements is to ensure that the operation of the power grid is not affected by wind farms in terms of protection of supply, reliability, and quality of power. A variety of experiments have been carried out over the past years to enhance the Fault Ride Through (FRT) capability of the DFIG wind turbine using different techniques [4].

FRT capability can be improved using three different methods, such as the installation of reactive power injection systems under transient conditions, protection circuits, and the deployment of controllers both under steady-state and transient conditions. Using the protection circuits and various controllers, it is possible to restrict over-current and surplus DC-link voltage produced by the rotor during grid disturbance [3-4]. Besides, the reactive power-injection system exceeds any reactive power deficit to improve the transient output of the DFIG based WT and to automatically align the rotor current and the DC-link voltage [4]. In this paper work, two methods are utilized to improve fault ride through capability of DFIG. The crowbar protection system is first employed to observe how the machine performs during a grid fault condition and later on for better enhancement of fault ride-through capability crowbar integrated with the BESS is analyzed. Figure 1(a) indicates the variable-speed configurations with reduced-capacity converters [5] and Figure 1(a) described the system with the intended crow bar connections.

Power converters

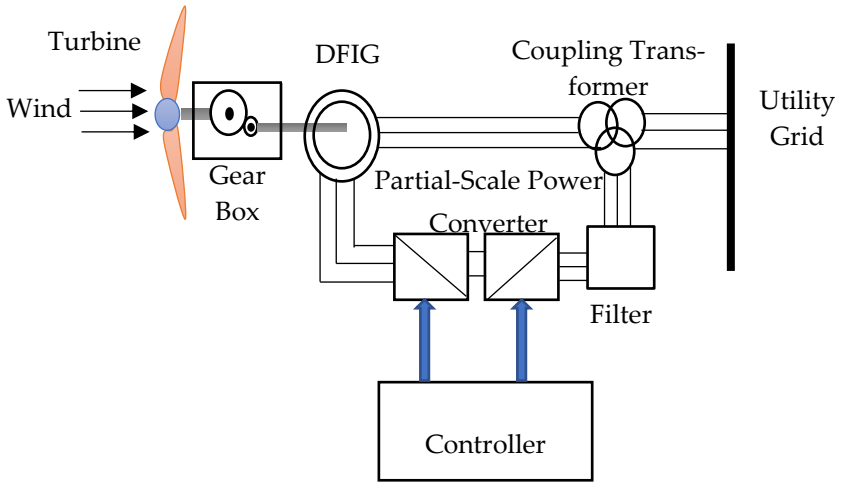

(a)

Preprints (www.preprints.org) | NOT PEER-REVIEWED | Posted: 21 July 2021 doi:10.20944/preprints202107.0476.v1

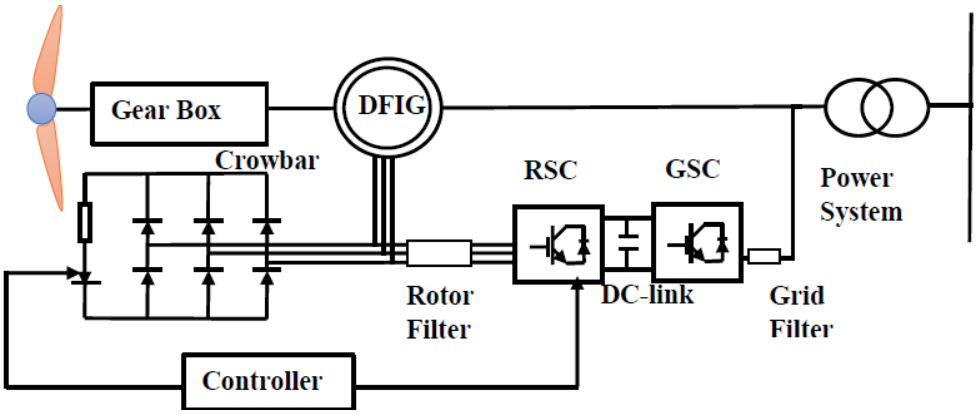

(b)

Figure 1. (a) variable-speed system with dual converters (b) Crowbar protection system

1.1. Related Work

Several researchers have employed various methods such as Crowbars, DC-Choppers, Series Dynamic Resistors (SDRs), Static synchronous compensator (STATCOM), Dynamic Voltage Restorer (DVR), Super Capacitors (SC), and Energy Storage Systems (ESSs) to improve FRT capability [6-7]. To enhance FRT capabilities, the authors in [6] proposed a crowbar protection method. When a fault occurs, a high stator and rotor current is generated, resulting in a high DC-link voltage. When the crowbar is engaged, it creates a low-resistance path that allows high currents to travel through it. However, because the rotor side converter is blocked during crowbar activation, control over speed and torque is lost, and torque is observed to fluctuate, causing mechanical stress on the drive train. Furthermore, when crowbar is turned on, the DFIG becomes a squirrel cage induction generator, collecting reactive power from the grid and further weakening it. The authors in [7] recommend employing a crowbar in combination with additional protective mechanisms such as SDR and SC for better enhancement of LVRT capability. The authors stated that when the crowbar is activated inhibiting the RSC for safety purposes, the speed and torque control of the machine is lost. Thus, by utilizing the crowbar with SDR it is possible to maximize the operation time of the RSC, thereby reducing torque fluctuation. SDR can also retain the current during disturbance and reduce the frequent use of crowbar. The DC link-chopper is another LVRT safety circuit that is discussed in depth in [8]. DC-chopper is a resistance circuit linked in parallel to the DC-link capacitor. This braking resistor, connected in series with the converter is used to maintain the DC-link voltage within acceptable operating voltage. However, after a fault, this method takes a longer time than the crowbar protection system to disengage the converter and return to normal operation. The authors in [11] have proposed DVR to mitigate sags, swells, and other power quality issues there by improving the FRT mechanism. This approach, however, has the downside of being costly, increasing the device complexity and expense while jeopardizing the reliability of the DFIG system. In [10], STATCOM is proposed in order to improve the performance of the machine during transient condition. STATCOM injects maximum reactive current to stabilize the electrical grid, accelerating voltage recovery and maintaining voltage stability. Furthermore, it also can generate both lagging and leading reactive power. However, STATCOM is quite expensive. The authors in [9] claim that the battery energy storage system is critical for sustaining a steady DC-link voltage. When the produced power taken from the wind system is more than the average power, it is frequently utilized to store energy at higher wind speeds. Furthermore, when the wind speed is lower and electricity from the grid is necessary, the battery drains and supplies the required power to the system, resulting in a constant DC-link voltage and a reliable and efficient grid supply. The authors, on the other hand, overlooked the fact that BESS can only maintain the DC-link voltage and has no control over the currents. As a result, an extra protective mechanism is required to prevent currents from harming the power converters. This

Preprints (www.preprints.org) | NOT PEER-REVIEWED | Posted: 21 July 2021 doi:10.20944/preprints202107.0476.v1

paper integrates the crowbar protection system with BESS for the crowbar to restrict the currents from damaging the converters and for BESS to maintain the DC-link voltage constant. Furthermore, combining BESS with crowbar can eliminate the shortcoming of crowbar protection systems, which is the loss of control and the machine's failure to deliver reactive power.

Table 1 Comparative analysis of different methods employed by to improve FRT capability

Ref	Methods	Merits	Demerits
[6]	Crowbar	Protects the power converter by restricting the currents.	Control over torque is lost. DFIG do not supply reactive power to the grid
[7]	Crowbar with SDR and SC	Maximizes the operating time of RSC so control will not be lost	voltage output in the protection scheme was unsatisfactory.
[8]	DC-chopper	maintain DC-link voltage by dissipating excessive energy	the time taken for restoration is longer than crowbar protection system
[9]	BESS	The DC-link voltage can be maintained constant	BESS can only maintain the DC-link voltage and do not have control over the currents
[10]	STATCOM	Support the voltage at the grid terminal by providing reactive power to the grid.	Higher cost
[11]	DVR	mitigate sags, swells, and other power quality issues there by improving the FRT mechanism.	costly, increasing the device complexity and expense while jeopardizing the reliability of the DFIG system.

1.2. Significance of the research

The main objective of this paper is to improve the FRT capability or performance of the machine during transient condition. The proposed method to achieve the objective of this work is crowbar integrated with BESS. Integrating crowbar with BESS eradicates the drawback that the crowbar has and improves the performance of the machine. When using a merely crowbar, as already discussed in section 1.1, the control over torque is lost and the machine does not deliver a reactive power to the grid. Thus, by combining the crowbar with BESS the performance of the machine can be improved in such a way that the BESS can maintain the DC-link voltage constant, provide reactive power to the grid, reduces the torque fluctuation and restore control over torque more promptly.

2. Fault Ride Through Capability Analysis of Wind Turbine with Doubly Fed Induction Generator

Fault ride-through capability refers to the capability of the generator to stay attached to the grid during voltage dips and swells. When a transient failure incident occurs, LVRT provisions mandate generation facilities to maintain contact to the grid network to provide post fault voltage [12]. The following sections describes the two FRT schemes used in this paper to improve the transient response of DFIGs-based wind turbines.

2.1. Crowbar Protection

Crowbar is a protection mechanism used to protect the power converters against high currents that arises due to grid faults by creating a low resistance path and by allowing the high currents flow through it [13]. Once the stator and rotor currents decay and the power converters gain control of the machine, the crowbar is deactivated. In crowbar protection system, the activation timing of crowbar and the value of resistance is critical. To fulfill the purpose of converter protection, the crowbar must be activated for an appropriate time [14]. When choosing the value of crowbar resistance, two major issues have to be

Preprints (www.preprints.org) | NOT PEER-REVIEWED | Posted: 21 July 2021 doi:10.20944/preprints202107.0476.v1

considered. If a high value of resistance is selected, large peak of electromagnetic torque will occur and with a low value resistance large currents are observed. Thus, appropriate value of resistance must be selected. The main concern with this protection method however is that continuous use of the rotor crowbar causes loss of control over the torque and the DFIG to operate as a squirrel cage induction machine and draw stator side magnetization. This results in a high-slip reactive power demand, which degrades stator voltage.

2.2. Battery Energy Storage System

During a fault, a voltage dip at the grid terminal prohibits the grid side converter from transferring power to the grid. Thus, excess energy is deposited in the DC-link capacitor, resulting in DC-link overvoltage. To prevent this issue, BESS is integrated with a crowbar to maintain a DC-link voltage constant [15]. Furthermore, the main drawback of the crowbar system is that, while it protects the RSC by ensuring that high currents circulate through it, machine control is lost due to RSC inhibition, and the DFIG operates like a squirrel cage induction generator, only absorbing reactive power from the grid, resulting in grid voltage degradation. As a result, integrating BESS with crowbar protection is crucial since during a failure, the stored energy in the battery discharges, supplying power to the GSC [16].

3. Modelling of Doubly Fed Induction Generator

This section presents a dynamic model of DFIG-based wind turbine to gain full insight into the dynamics performance of the system and to design the control system in any particular situations [17].

3.1. Dynamic Model of Doubly Fed Induction Generator

A dynamic model can provide the continuous performance of the variables of the machine, such as torque, currents, and fluxes, under certain voltage supply conditions. In that way, it is possible to identify dangerous behaviors, such as volatility or strong transient currents by identifying the transition from one state to another [18].

3.1.1. α, β Model

For simplification purpose, it is essential to transform three-phase machines into two-phase stationery, rotor, and synchronous reference frame as shown in Figure 2 [19].

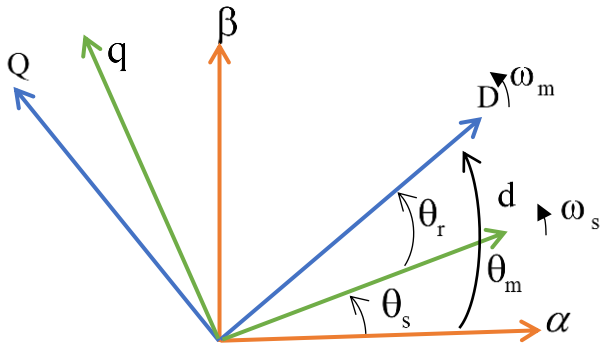

Figure 2. Different reference frames to represent space vectors of the DFIM [19]

Stator and rotor voltage, stator and rotor flux, active and reactive power, and torque in (α, β) is given as:

$$v_{\alpha s} = R_s i_{\alpha s} + \frac{d\psi_{\alpha s}}{dt}$$
$$v_{\beta s} = R_s i_{\beta s} + \frac{d\psi_{\beta s}}{dt} \quad (1)$$

Preprints (www.preprints.org) | NOT PEER-REVIEWED | Posted: 21 July 2021 doi:10.20944/preprints202107.0476.v1

$$v_{\alpha r} = R_r i_{\alpha r} + \frac{d\psi_{\alpha r}}{dt} + \omega_m \psi_{\beta r}$$
$$v_{\beta r} = R_r i_{\beta r} + \frac{d\psi_{\beta r}}{dt} - \omega_m \psi_{\alpha r} \quad (2)$$

$$\psi_{\alpha s} = L_s i_{\alpha s} + L_m i_{\alpha s}$$
$$\psi_{\beta s} = L_s i_{\beta s} + L_m i_{\beta s} \quad (3)$$

$$\psi_{\alpha r} = L_m i_{\alpha r} + L_r i_{\alpha r}$$
$$\psi_{\beta r} = L_m i_{\beta r} + L_r i_{\beta r} \quad (4)$$

$$P_s = 1.5(v_{\alpha s} i_{\alpha s} + v_{\beta s} i_{\beta s})$$
$$Q_s = 1.5(v_{\beta s} i_{\alpha s} - v_{\alpha s} i_{\beta s}) \quad (5)$$

$$P_r = 1.5(v_{\alpha r} i_{\alpha r} + v_{\beta r} i_{\beta r})$$
$$Q_r = 1.5(v_{\beta r} i_{\alpha r} - v_{\alpha r} i_{\beta r}) \quad (6)$$

$$T_{em} = 1.5\left(\frac{L_m}{\sigma L_r L_s}\right) p\, \mathrm{Im}\{\psi_r . \psi_s\} \quad (7)$$

Where, $V_{\alpha s}$, $V_{\alpha R}$, V_{Bs}, V_{Br}, $I_{\alpha s}$, $I_{\alpha r}$, I_{Bs}, I_{Br}, and $\Psi_{\alpha s}$, $\Psi_{\alpha r}$, Ψ_{Bs}, Ψ_{Br} are voltages, currents and flux linkages of the stator and rotor in α, β axis respectively. R_s and R_r are the stator and rotor resistances, L_s and L_r and L_m are the stator, rotor, and mutual inductance respectively, ω_m and ω_s are the rotor electrical speed and the stator frequency, P_s, P_r, Q_s and Q_r are the active and reactive powers of the stator and rotor of the DFIG in the (α, β) frames, P is the pole pair of the machine and $\sigma = (1 - L_m^2) / (L_s - L_r)$ is the leakage coefficient.

3.1.2. d-q Model

The stator and rotor voltage and stator and rotor flux in the d-q reference frame is expressed as:

$$v_{ds} = R_s i_{ds} + \frac{d\psi_{ds}}{dt} - \omega_s \psi_{qs}$$
$$v_{qs} = R_s i_{qs} + \frac{d\psi_{qs}}{dt} + \omega_s \psi_{ds} \quad (8)$$

$$v_{dr} = R_r i_{dr} + \frac{d\psi_{dr}}{dt} - \omega_r \psi_{qr}$$
$$v_{qr} = R_r i_{qr} + \frac{d\psi_{qr}}{dt} + \omega_r \psi_{dr} \quad (9)$$

$$\psi_{ds} = L_s i_{ds} + L_m i_{dr}$$
$$\psi_{qs} = L_s i_{qs} + L_m i_{qr} \quad (10)$$

$$\psi_{dr} = L_r i_{dr} + L_m i_{ds}$$
$$\psi_{qr} = L_r i_{qr} + L_m i_{qs} \quad (11)$$

Where, $V_{ds}, V_{dr}, V_{qs}, V_{qr}$, $i_{ds}, i_{dr}, i_{qs}, i_{qr}$ and $\psi_{ds}, \psi_{dr}, \psi_{qs}, \psi_{qr}$ are voltages, currents, and flux linkages of the stator and rotor in the d-q axis.

Preprints (www.preprints.org) | NOT PEER-REVIEWED | Posted: 21 July 2021 doi:10.20944/preprints202107.0476.v1

4. Control System for Doubly Fed Induction Generator

The control strategy utilized in this study for controlling DFIG is vector-oriented control in the synchronous reference frame. It has numerous pros such as a good dynamic response, robust to parameter variation and measurement noise, and a set switching frequency [20-21].

4.1. Rotor Side Control

The RSC has the ability to control the active and reactive power separately by regulating the rotor current. The direct rotor current is aligned with the stator flux orientation as shown in Figure 3 which enables the active and reactive power control by regulating the d-axis and q-axis rotor current [20].

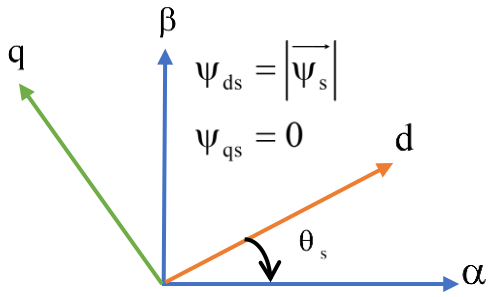

Figure 3. Vector control of the d-q reference aligned with stator flux space vector [21]

The flux, current and voltage in d-q axis is given as:

$$\psi_{ds} = \psi_s = i_{ds}L_s + i_{dr}L_m$$
$$0 = i_{qs}L_s + i_{qr}L_m \quad (12)$$

$$i_{ds} = \frac{1}{L_s}(\psi_s - L_m i_{dr})$$
$$i_{qs} = -\frac{L_m}{L_s} i_{qr} \quad (13)$$

$$\psi_{dr} = \frac{L_m}{L_s}\psi_{ds} + \sigma L_r i_{dr}$$
$$\psi_{qr} = \sigma L_r i_{qr} \quad (14)$$

Where, σ is $(1-\frac{L_m^{\ 2}}{L_s})$

In the absence of a small drop in stator resistance, the voltage of the stator and the relationship between the voltage of the rotor and the current can be expressed as follows:

$$v_{ds} = 0$$
$$v_{qs} = v_g = \omega_s \psi_s \quad (15)$$

$$v_{dr} = R_r i_{dr} - \omega_r \sigma L_r i_{qr} + \sigma L_r \frac{d}{dt} i_{dr}$$
$$v_{qr} = R_r i_{qr} + \omega_r \sigma L_r i_{dr} + \sigma L_r \frac{d}{dt} i_{qr} \quad (16)$$

Preprints (www.preprints.org) | NOT PEER-REVIEWED | Posted: 21 July 2021 doi:10.20944/preprints202107.0476.v1

The stator active, reactive power and the electromagnetic torque can be written as:

$$P_s = -\frac{3L_m}{2L_s}(v_{qs}i_{qr}) \tag{17}$$

$$Q_s = \frac{3v_{qs}}{2L_s}(\psi_{ds} - L_m i_{dr}) \tag{18}$$

$$T_e = -\frac{3}{2}p\frac{L_m}{L_m}(\psi_{ds}i_{qr}) \tag{19}$$

The rotor angle is obtained from (20)

$$\begin{aligned} \theta_v &= \tan^{-1}\left(\frac{v_\beta}{v_\alpha}\right) \\ \theta_s &= \theta_v - 90^0 \\ \theta_r &= \theta_s - (p.\theta_m)_{elec} \end{aligned} \tag{20}$$

4.2. Grid Side Control

GSC is used to control the DC-link voltage and provides reactive support to the grid as demanded by the grid codes [18]. A voltage-oriented vector control is utilized for the control of the machine. The d-axis rotor current is used to regulate the DC-link voltage and the q-axis current is used to regulate the reactive power [21].

The balance across the inductor is as follows:

$$\begin{bmatrix} v_{ag} \\ v_{bg} \\ v_{cg} \end{bmatrix} = R_g \begin{bmatrix} i_{ag} \\ i_{bg} \\ i_{cg} \end{bmatrix} + L_g \frac{d}{dt}\begin{bmatrix} i_{ag} \\ i_{bg} \\ i_{cg} \end{bmatrix} + \begin{bmatrix} v_{ag\_conv} \\ v_{bg\_conv} \\ v_{cg\_conv} \end{bmatrix} \tag{21}$$

Where, i_{ag}, i_{bg}, i_{cg} indicates the three-phase grid-side converter currents, V_{ag}, V_{bg}, V_{cg} are the three-phase grid voltages, $V_{ag\_conv}, V_{bg\_conv}, V_{cg\_conv}$ are the three-phase grid-side converter voltages, R_g and L_g are the inductor resistance and inductance respectively.

Converting the three-phase in to two phase stationary and rotating reference frame (α, β and d-q)

$$\begin{aligned} v_{\alpha g} &= R_g i_{\alpha g} + L_g \frac{di_{\alpha g}}{dt} + v_{\alpha g\_conv} \\ v_{\beta g} &= R_g i_{\beta g} + L_g \frac{di_{\beta g}}{dt} + v_{\beta g\_conv} \end{aligned} \tag{22}$$

Preprints (www.preprints.org) | NOT PEER-REVIEWED | Posted: 21 July 2021 doi:10.20944/preprints202107.0476.v1

$$v_{dg} = R_g i_{dg} + L_g \frac{di_{dg}}{dt} - \omega_e L_g i_{qg} + v_{dg\_conv}$$
$$v_{qg} = R_g i_{qg} + L_g \frac{di_{qg}}{dt} + \omega_e L_g i_{dg} + v_{qg\_conv} \quad (23)$$

Where, V_{dg}, V_{qg} are the grid voltages in d-q axis, V_{dg_conv}, V_{qg_conv} are the grid-side converter voltages in d-q axis, i_{dg}, i_{qg} are the grid-side converter currents in d-q axis, ω_e is the electrical angular velocity of the grid voltage.

The active and reactive power is expressed as:

$$P_g = 1.5\left(v_{dg} i_{dg} + v_{qg} i_{qg}\right)$$
$$Q_g = 1.5\left(v_{qg} i_{dg} - v_{dg} i_{qg}\right) \quad (24)$$

The angular position of the supply voltage is computed as follows:

$$\theta_e = \int \omega_e dt = \tan^{-1}\left[\frac{v_{\beta g}}{v_{\alpha g}}\right] \quad (25)$$

4.3. Maximum Power Point Tracking Control

At the point when the wind speed is over the cut-in speed and below the rated speed, the speed control is fundamental as it ceaselessly adjusts the speed of the rotor to sustain the tip speed ratio steady at the level that provides ideal power coefficient and high proficiency. The speed control strategy used in this work is indirect speed control. The indirect speed control relies upon the association between the electromagnetic torque and the angular velocity [22].

5. Results and Discussions

This section presents a simulation analysis to evaluate the performance of DFIG during three phase symmetrical fault conditions. During a failure condition, simulation results are first assessed with just a crowbar protection, and then with a crowbar combined with BESS to enhance the operational performance of the machine and meet grid code criteria.

5.1. Under Grid Fault Condition with the Crowbar

The subsequent section presents how DFIG operates during three-phase symmetrical fault condition with crowbar protection system employed.

5.1.1. RSC Under Grid Fault Condition with Crowbar Protection System

As depicted in Figure 5 (a), the voltage dropped to 0.1 pu and remained at that level for 150 ms. When the voltage drop is identified, the crowbar protection is triggered for 100 milliseconds to block RSC by enabling the high currents to travel through the crowbar and protect the converter against excessive currents. Figure 5 (c, d, e) illustrates that the high stator and rotor currents flows through the crowbar. The torque and flux, as illustrated in Figure 5 (b, f), are impacted by the grid fault. The flux and the torque are observed to be reduced to zero. In Figure 5 (b), it is recognized that the torque does not reach the reference value even after the error has been removed. This is due to the fact that when the crowbar is activated, torque control is lost and up to 5 sec the torque control is not recovered. Once the flux and torque return to its rated value and the converter control is gained, the crowbar is deactivated. The d-axis and q-axis rotor current is shown in

Preprints (www.preprints.org) | NOT PEER-REVIEWED | Posted: 21 July 2021 doi:10.20944/preprints202107.0476.v1

Figure 5 (g, h). When a dip occurs, increasing d-axis rotor current, as required by grid code, will gradually supply reactive power via the stator. However, no reactive power can be achieved during the activation of crowbar as the crowbar blocks the RSC. Consequently, reactive power is delivered through the stator only after some time (2.14 seconds).

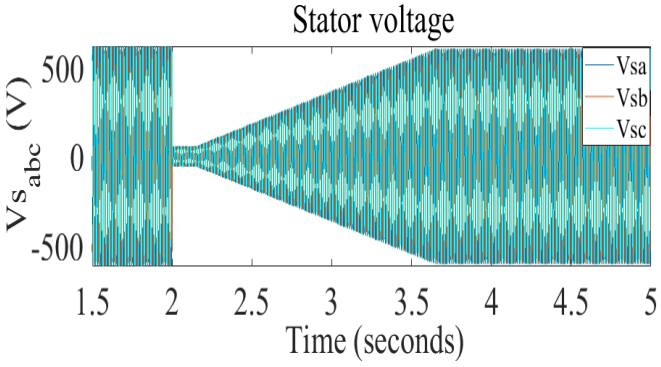

(a) Stator voltage

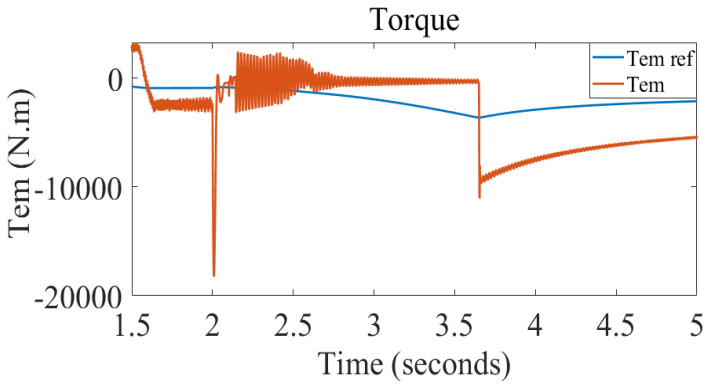

(b) Torque

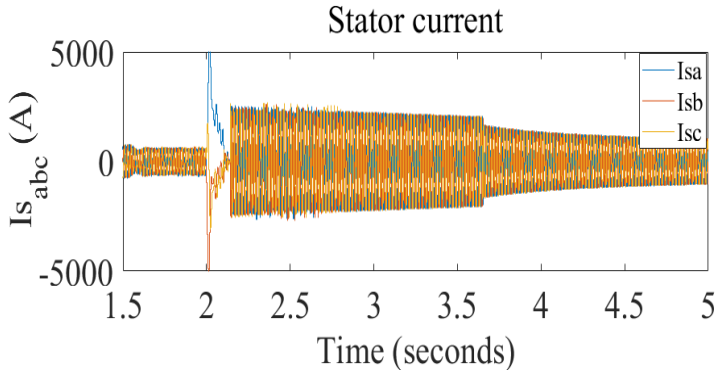

(c) Stator current

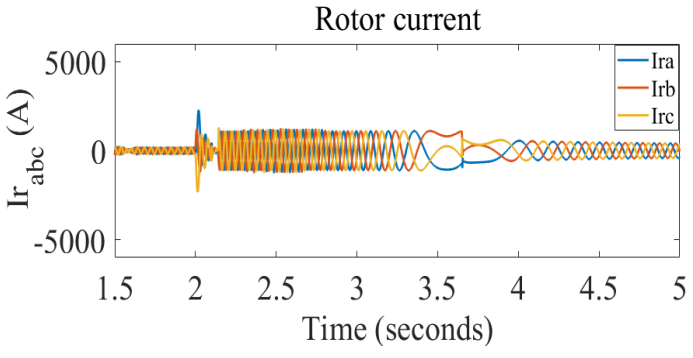

(d) Rotor current

Preprints (www.preprints.org) | NOT PEER-REVIEWED | Posted: 21 July 2021 doi:10.20944/preprints202107.0476.v1

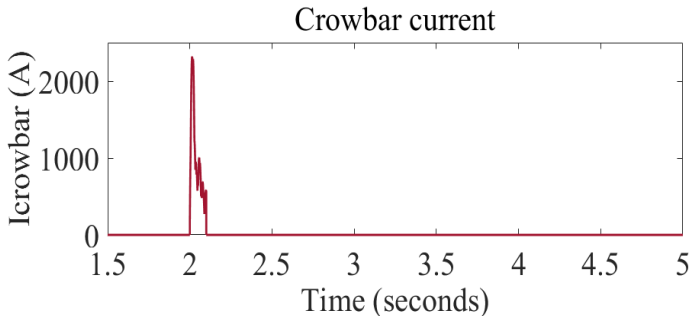

(e) Crowbar current

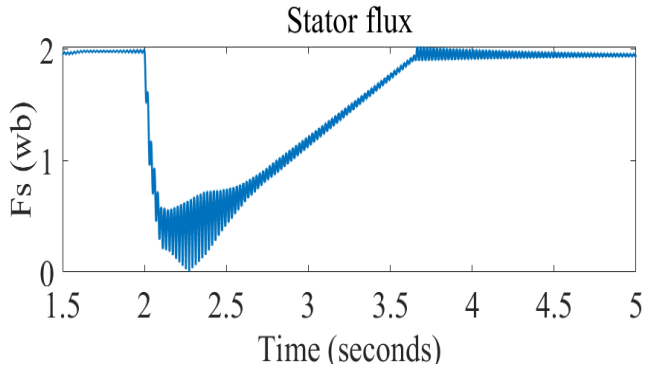

(f) Stator flux

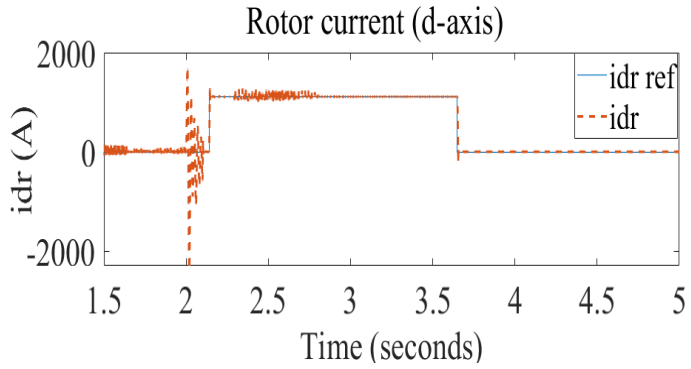

(g) Rotor current (d-axis)

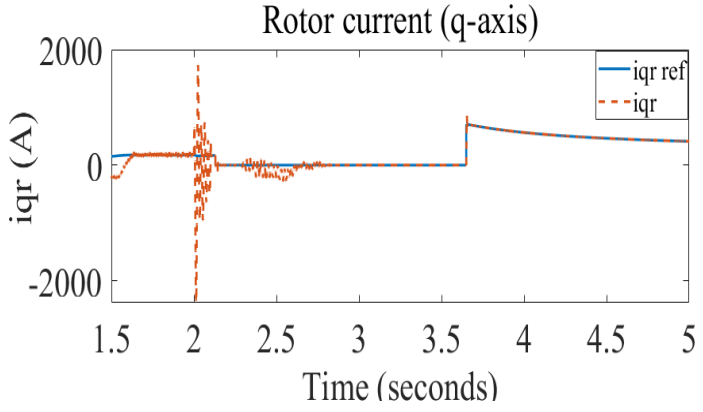

(h) Rotor current (q-axis)

Preprints (www.preprints.org) | NOT PEER-REVIEWED | Posted: 21 July 2021 doi:10.20944/preprints202107.0476.v1

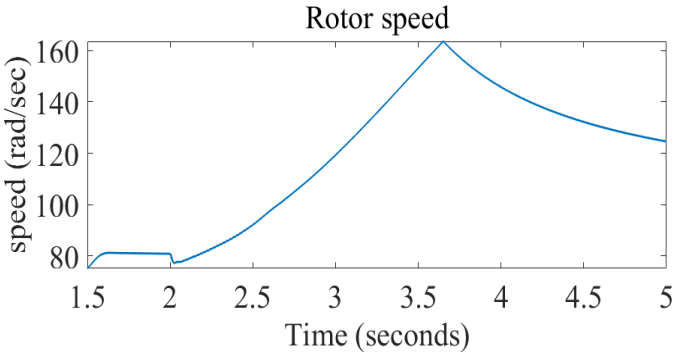

(i) Rotor speed

Figure 4. Performance of DFIG with crowbar at RSC

5.1.2. GSC Under Grid Fault Condition with Crowbar Protection System

Due to the restricted value of the rotor voltage that the power converter generates, the GSC loses its capacity in the event of a malfunction. Through the use of the protective mechanism at time the control is lost, the performance of DFIG at the GSC is assessed. Figure 6(a) shows how the grid current after activation of the crowbar is kept constant. Figure 6(b) indicates that no energy is transmitted to the DC-link capacitor when Crowbar is activated and hence the DC-link voltage drops. However, the DC-link voltage is found to be back into stable condition once the crowbar is disabled and the fault is removed. After the fault clearance the grid current across d-axis and q-axis as shown in Figure 6 (c, d) remains at its nominal value.

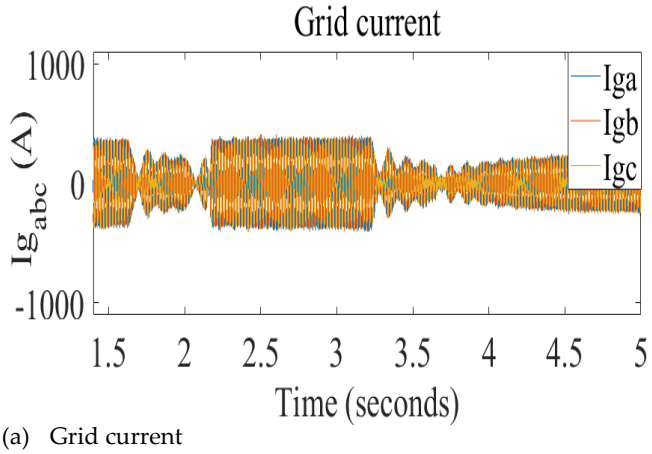

(a) Grid current

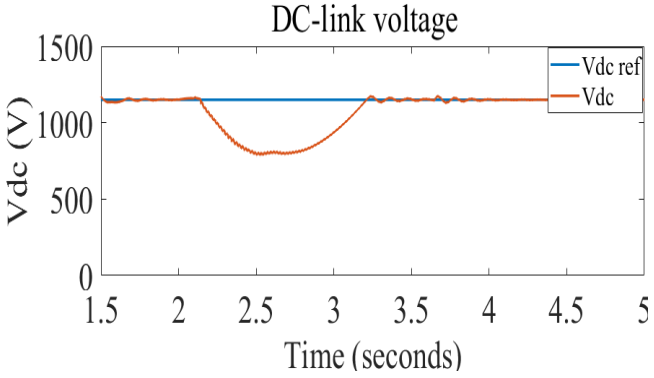

(b) DC-link voltage

Preprints (www.preprints.org) | NOT PEER-REVIEWED | Posted: 21 July 2021 doi:10.20944/preprints202107.0476.v1

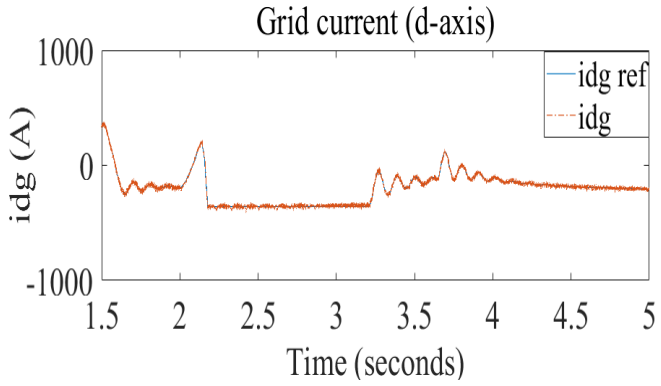

(c) Grid current (d-axis)

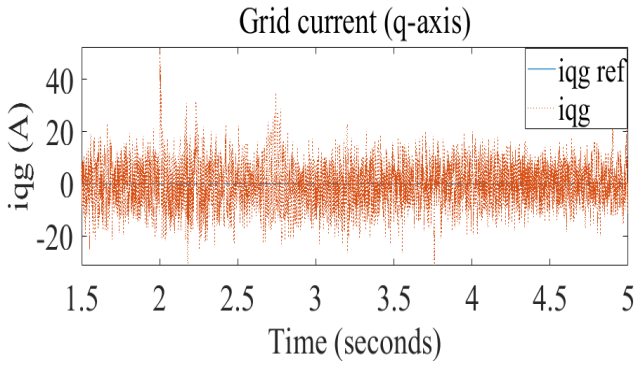

(d) Grid current (q-axis)

Figure 5. Performance of DFIG with crowbar at GSC

5.2. Under Grid Fault Condition with Crowbar Protection Integrated with BESS

Although the crowbar protection system is critical for securing the converters, it has some drawbacks. The negative aspect of the crowbar system is that, while it protects the RSC by ensuring the high currents flow through it, machine control is lost as a consequence of RSC inhibition. Besides, the DFIG acts like a squirrel cage induction generator, only absorbing reactive power from the grid, resulting in grid voltage degradation. As a result, BESS implementation is vital since, in the event of a loss, the stored energy in the battery discharges, powering the GSC.

5.2.1. RSC Under Grid Fault Condition with Crowbar Protection Integrated with BESS

By incorporating BESS with Crowbar, the BESS ensures that control over the machine is not lost. When the crowbar is enabled, speed and torque control is lost because the crowbar blocks the RSC. As seen in Figure 7 (c, i), once the BESS is merged with the protection system, after some time, the speed observed to return to its normal operation. Following the reference value, the torque is also retained at its nominal value. As displayed in Figure 5 (g), raising the direct current provides for reactive power only after the crowbar was disabled. However, when BESS is integrated with crowbar, as depicted in Figure 7 (d), even with crowbar protection stimulated, BESS allows reactive power to be supplied via the stator, which improves the performance of the machine. Figure 7 (b, f, g) indicates how the high value of stator and rotor current enters the crowbar.

Preprints (www.preprints.org) | NOT PEER-REVIEWED | Posted: 21 July 2021 doi:10.20944/preprints202107.0476.v1

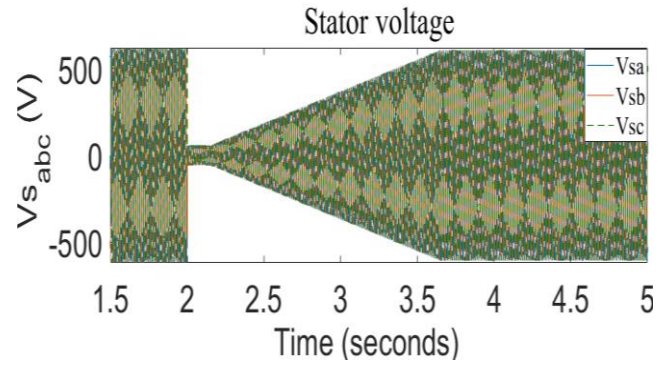

(a) Stator voltage

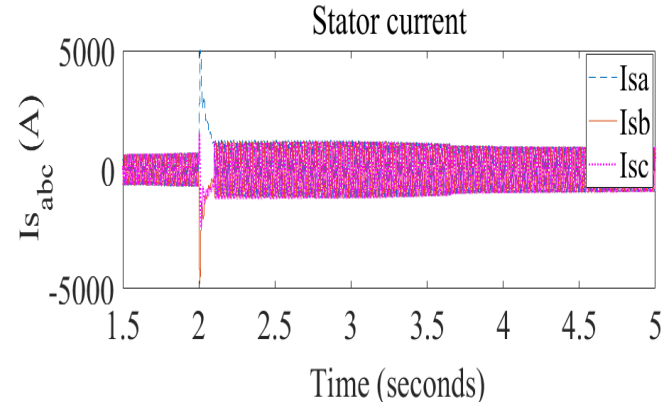

(b) Stator current

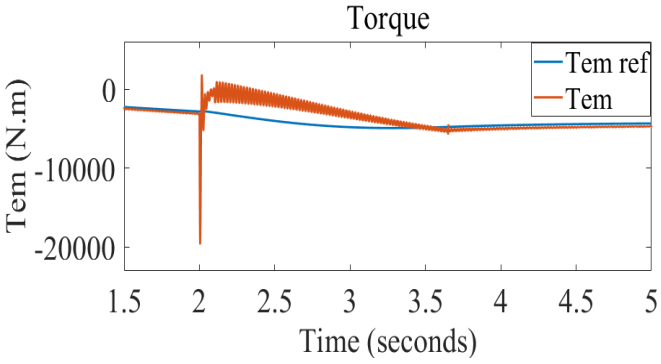

(c) Torque

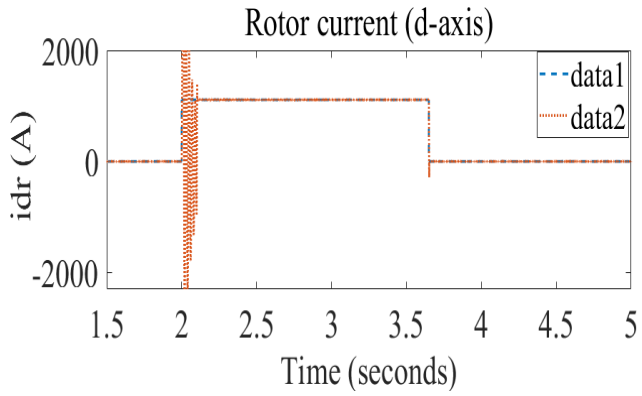

(d) Rotor current (d-axis)

Preprints (www.preprints.org) | NOT PEER-REVIEWED | Posted: 21 July 2021 doi:10.20944/preprints202107.0476.v1

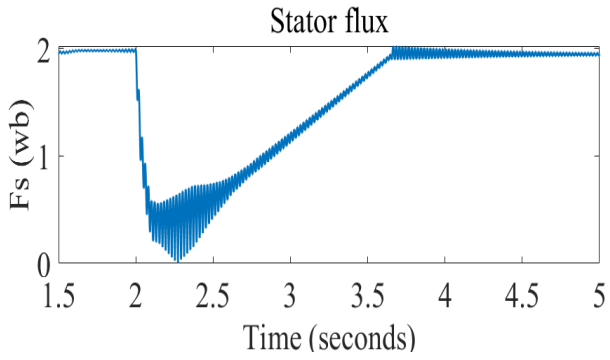

(e) (Stator flux

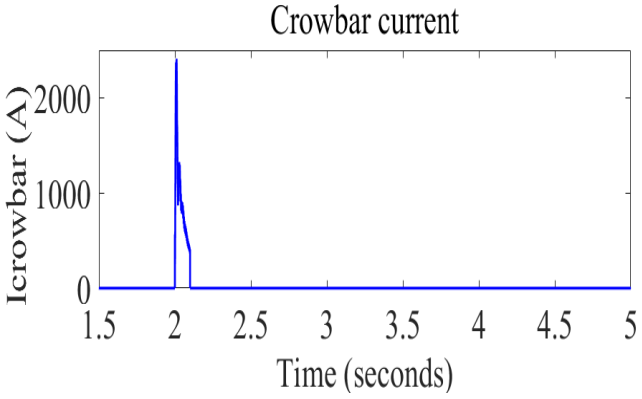

(f) Crowbar current

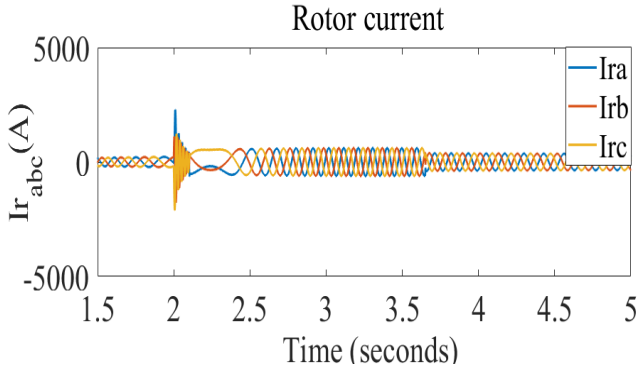

(g) Rotor current

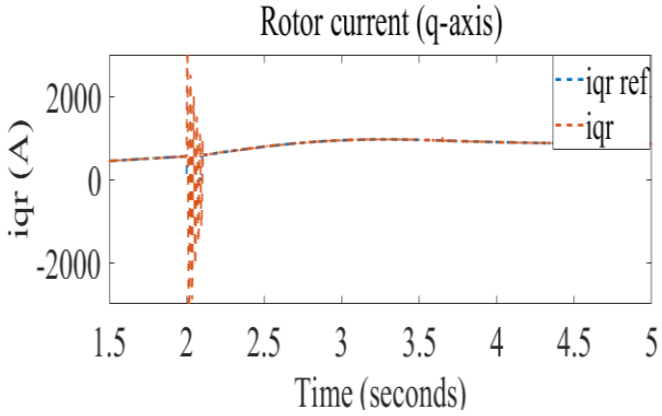

(h) Rotor current (q-axis)

Preprints (www.preprints.org) | NOT PEER-REVIEWED | Posted: 21 July 2021 doi:10.20944/preprints202107.0476.v1

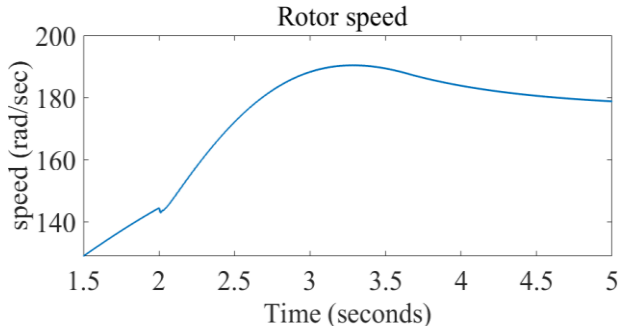

(i) Rotor speed

Figure 6. Performance of DFIG with crowbar integrated with BESS at RSC

5.2.2. GSC Under Grid Fault Condition with Crowbar Protection Integrated with BESS

The battery, following a power converter, aids in maintaining a constant DC bus voltage. Figure 8 (a, b) depicts that the grid current and DC-link voltage is nearly constant owing to the BESS. In Figure 8 (c), the grid current across the d-axis, which is in charge of regulating the DC-link voltage, is also shown to be constant. Figure 8 (d) illustrates that the grid currents across the q-axis remain stable.

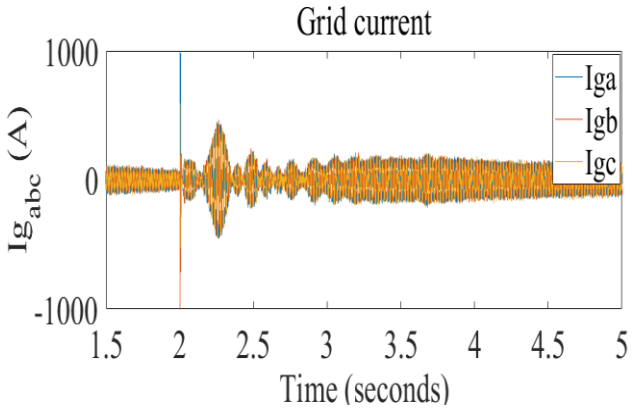

(a) Grid current

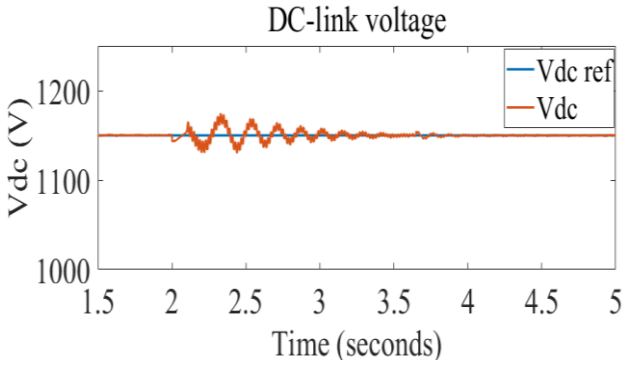

(b) DC-link voltage

Preprints (www.preprints.org) | NOT PEER-REVIEWED | Posted: 21 July 2021 doi:10.20944/preprints202107.0476.v1

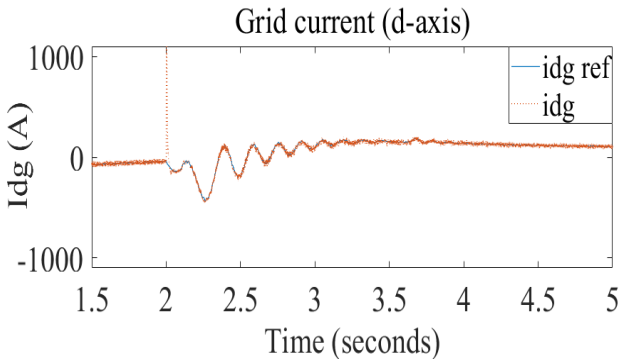

(c) Grid current (d-axis)

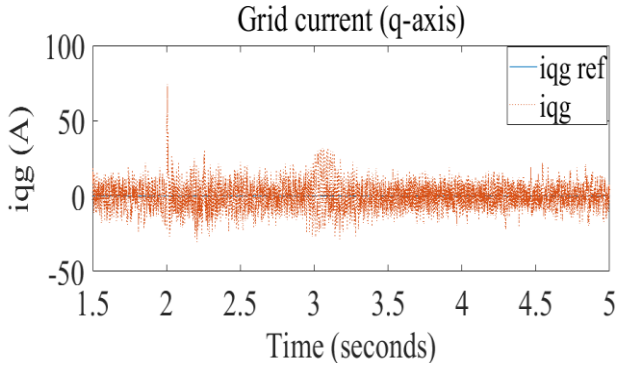

(d) Grid current (q-axis)

Figure 7. Performance of DFIG with crowbar integrated with BESS at GSC

5.3. Comparative Analysis of the Results

This section provides a thorough comparison of various parameters at the RSC and GSC with the crowbar protection mechanism, and crowbar integrated with BESS.

5.3.1. Comparative Analysis at RSC

A detail comparison of various parameters observed at RSC with the crowbar protection system, and crowbar incorporated with BESS is performed. Figure 9 illustrates various parameters at RSC which were used for comparative purposes. A distinct number is assigned to each figure in order to differentiate it. The parameters with the crowbar protection system are denoted by '1', and the parameters with the crowbar integrated with BESS are denoted by '2'. Figure 9 (a1, and a2) demonstrate the torque value with a crowbar protection, and crowbar integrated with BESS. Sub Figure (a1) displays that with the crowbar activated, even though the fluctuation of torque is minimized, control over torque is lost, and the torque takes time to follow the reference value even after the crowbar is deactivated. With the activation of crowbar, the value of torque is zero and it takes more than 5 sec for it to recover. However, in sub Figure (a2), the torque fluctuation is lowered to a considerably lower value, and the torque is likewise observed to restore to its nominal level after 3.4 seconds. The torque is observed to return to nominal value after 3.2 sec. Sub Figures (c1, d1, f1) and (c2, d2. f2) demonstrate that when the crowbar is activated, high currents flow through it. As a result, the converters are shielded from large currents caused by faults. In sub Figure (e1), it is proven that rising rotor current across d-axis to 1100A supplies reactive power to the grid; however, it is also noted that reactive power is given to the grid only after the crowbar is deactivated (i.e. 2.14sec). With a BESS integrated with crowbar, as shown in sub Figure (e2), the machine is observed to be delivering reactive power the instant the fault occurs at the grid terminal, which is 2 seconds.

Preprints (www.preprints.org) | NOT PEER-REVIEWED | Posted: 21 July 2021 doi:10.20944/preprints202107.0476.v1

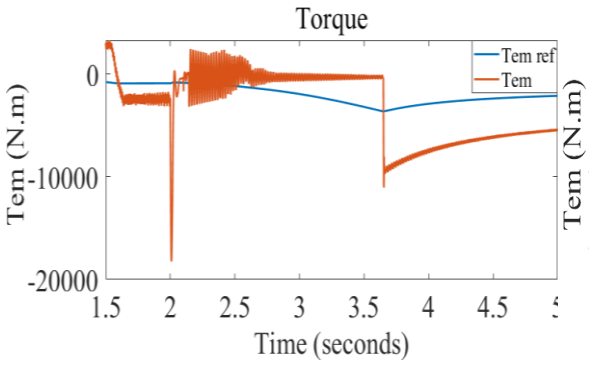

(a1)

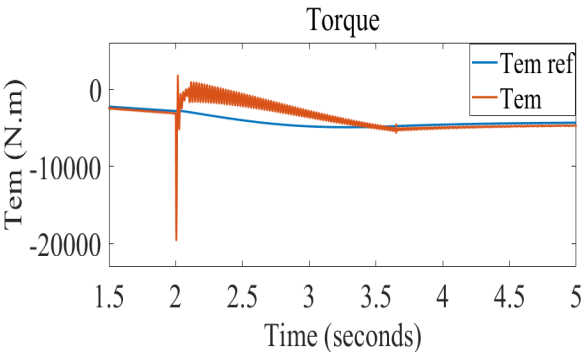

(a2)

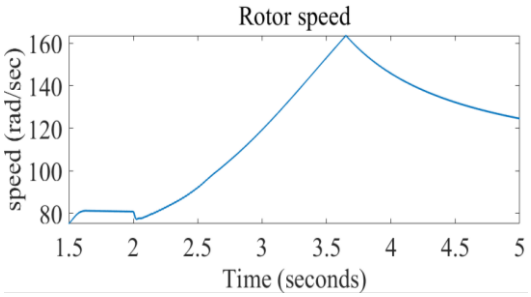

(b1)

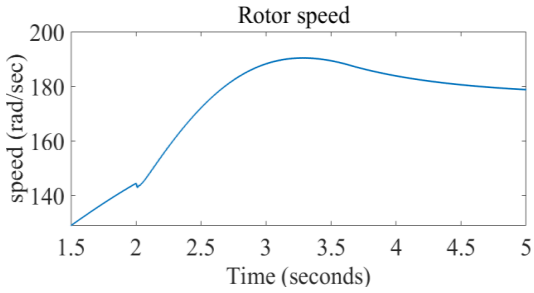

(b2)

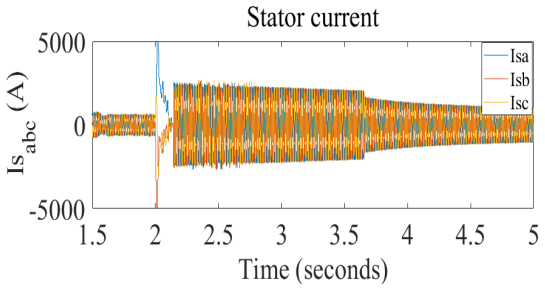

(c1)

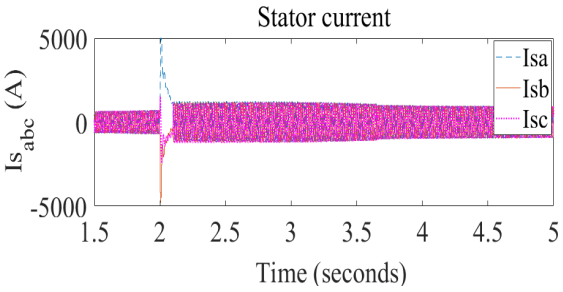

(c2)

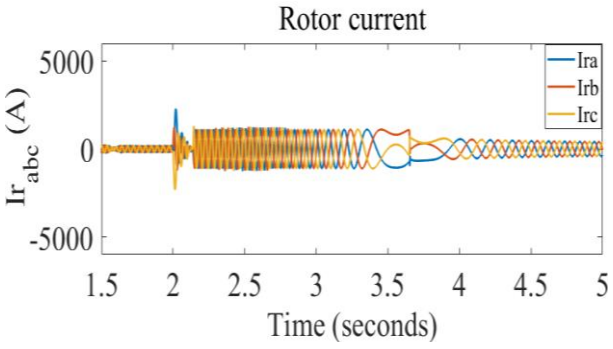

(d1)

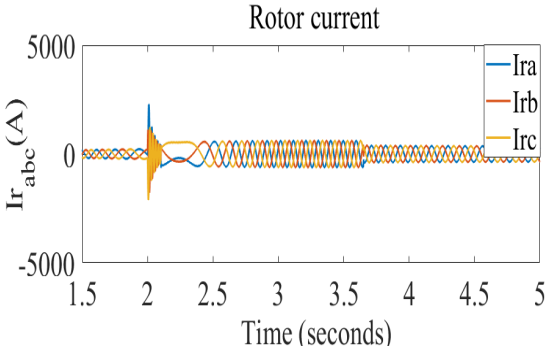

(d2)

Preprints (www.preprints.org) | NOT PEER-REVIEWED | Posted: 21 July 2021 doi:10.20944/preprints202107.0476.v1

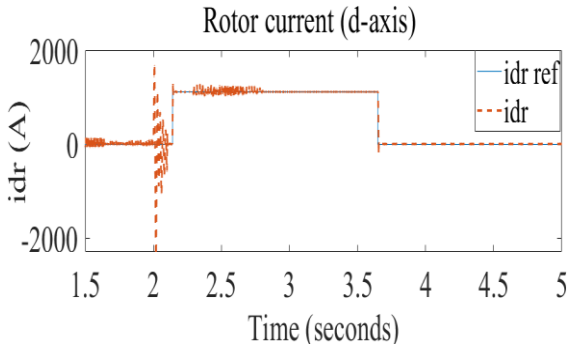

(e1)

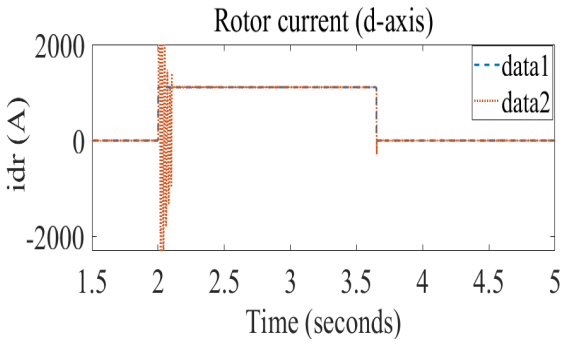

(e2)

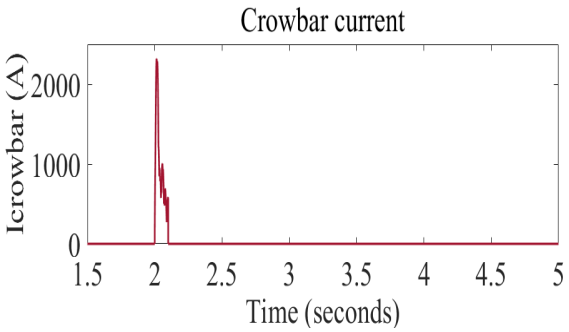

(f1)

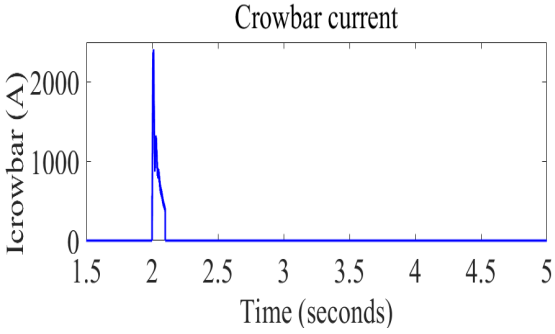

(f2)

Figure 8: Comparative analysis at RSC

5.3.2. Comparative Analysis at GSC

Figure 10 depicts a comparison of various parameters at GSC with a crowbar protection system, and crowbar merged with BESS. Sub Figure (a1, and a2) demonstrates the current at the grid side converter. In sub Figure (a2) the current at the grid terminal returns to normal around 2.6 seconds which is faster restoration than the crowbar protection. Sub Figure (b1) demonstrates that when the crowbar is utilized to the system, the dc-link voltage drops to a low level (775v). This is due to the fact that the crowbar prevents all energy from passing through the DC-link capacitor causing the DC-link voltage to drop. The lower value of DC-link voltage (775v) will result in power instability at the grid as the GSC can only supply less power stored in DC-link to the grid. Thus, in order to improve power stability, the DC-link voltage must be maintained constant.

In sub Figure (b2), with BESS combined with crowbar, the DC-link voltage is shown to remain at its nominal value (1150 V) with a small variation, and these fluctuations, which are totally removed after 2.5 sec, are not high enough to harm the power converters. As illustrated in sub Figure (c1), the d-axis grid current is observed to reduce to a value of -350A when the crowbar protection system is applied to the system and kept fluctuating even after crowbar is deactivated. Sub Figure (c2) depicts the current across the d-axis fluctuates for few seconds but later after 2.7second it is shown to settle down to its nominal value which is zero. Thus, with the proposed method (crowbar integrated with BESS) it is observed that fault ride through capability is enhanced.

Preprints (www.preprints.org) | NOT PEER-REVIEWED | Posted: 21 July 2021 doi:10.20944/preprints202107.0476.v1

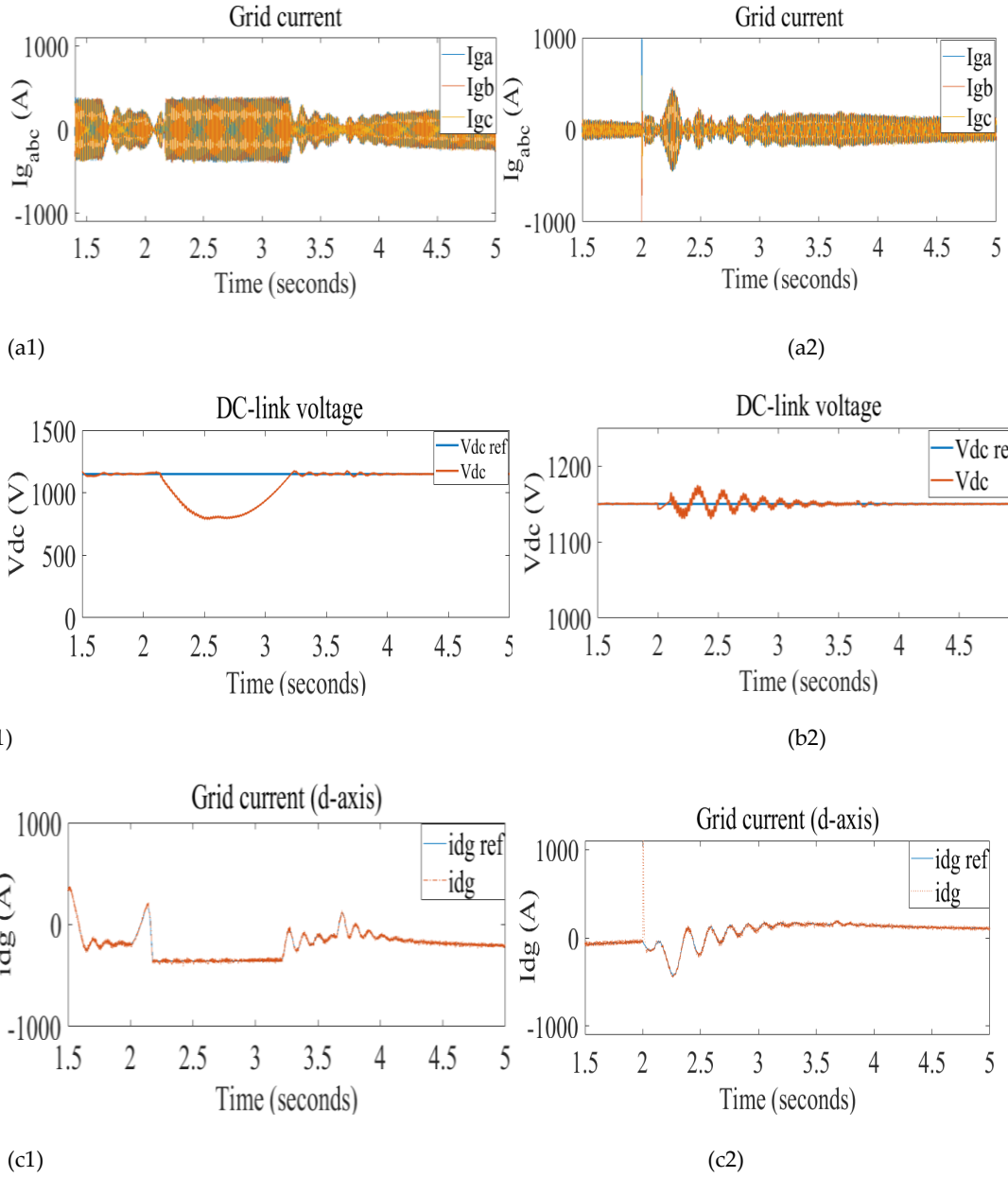

Figure 9. Comparative analysis at GS

 doi:10.20944/preprints202107.0476.v1

Table 2 comparative analysis of the result

	Crowbar protection	Crowbar integrated with BESS
Parameters	Values and settling time	
DC-link voltage	Voltage reduced to 775v and recovers after 3.45seconds	Voltage is maintained at 1150 with few fluctuations. Settles at 2.9 seconds
Grid current across the d-axis	The grid current kept fluctuating between -350 and -200 and even after 4.5 sec it does not settle down to its nominal value.	The fluctuation of grid current reduces and settles down to nominal value after 2.9 seconds
Rotor current across d-axis	Due to the activation of crowbar DFIG do not supply reactive power for 140ms. It can only supply after 2.14 seconds	Reactive power is provided to the grid at 2 seconds until the voltage completely recovers which is 3.65 seconds
Torque and speed	Control over the torque and speed is lost and didn't return to nominal value after 5 seconds	Fluctuation of the torque is reduced and the torque control recovers after 3.3 seconds. The speed also recovers after 3.5 sec.

The comparative analysis of the result is shown in Table 2. As a result of the comparison analysis, the suggested protection system outperforms the crowbar in terms of fault ride through capability. FRT capability refers to the ability of generator to stay connected to the grid even when there are faults. In this analysis the proposed method performs better in riding through the fault and safeguarding the machine from harm. For instance, the settling time for DC-link voltage using simply a crowbar protection system is 3.45 seconds, whereas the settling time utilizing the suggested technique is 2.9 seconds. This implies that the system rides the fault quickly and preserve its nominal value. As a result, the suggested technique outperforms relying just on the crowbar protection mechanism.

6. Conclusion

A severe grid terminal fault causes reduced stator and rotor flux, increased stator and rotor current, which may influence the converter, DC-link overvoltage, and torque fluctuation, which increases mechanical tension. In order to solve this issue, the crowbar protection is integrated with BESS. The proposed scheme is contrasted to a crowbar to demonstrate the effectiveness of the outcome. The use of a crowbar protects the power converters from being damaged by the high stator and rotor currents. However, since it blocks all energy, the dc-link voltage drops to 775 volts. The lower the voltage, the more power instability there is on the grid. Furthermore, the simulation results show that when the crowbar protection mechanism is used, the machine does not provide reactive power to the grid. Reactive power is provided by raising the rotor current across the d-axis only after 2.14 seconds. As a result, to address this problem the proposed approach is utilized. The new approach was demonstrated to increase the performance of the machine over the previous one (crowbar). The DC-link voltage is nearly steady (1150v), the stator and rotor currents are regulated to appropriate levels, and the reactive power is fed to the grid by raising the current at the d-axis to a value of 1100A, as shown in the simulation results. At the instant the fault occurs, which is at 2 seconds, the machine is shown to deliver reactive power to the grid. As a result, merging crowbar protection with BESS enhances machine performance by quickly riding through faults, maintaining DC-link voltage constant, and delivering reactive power to the grid.

Funding: This research received no external funding.

Conflicts of Interest: The authors declare no conflict of interests

Appendix A

Table A: Wind Turbine and Controller parameters

Parameters	**Values**
Rated Power	1.5MW
Number of Pole Pairs	2
Rated Stator Line-to-line Voltage	690V
Rotor voltage of open circuit	1650V
Rated Stator Current	1110A
Frequency	50HZ
Rated speed	1800rpm
Speed range	1000-2000rpm
Cut-in speed	3.5m/s
Rated speed	12m/s
Cut-out speed	25m/s
Cpmax.	0.4865
Lambda opt	8.1
Rated Slip	0.2
Inertia	67
Gearbox ratio	94.7
Blade length	37m
Rotor diameter	77m
DC-link voltage	1150V
Kp_ir	2.2037
Kp_ig	0.3642
Kp_wn	5360
Ki_wn	21440
Kp_vdc	-1000
Ki_vdc	-300000
Kpg	0.0012
Kqg	-0.0012

References

1. L. Widanagama, Arachchige, A. Rajapakse, and D. Muthumuni, "Implementation, Comparison and Application of an Average Simulation Model of a Wind Turbine Driven Doubly Fed Induction Generator," *Energies*, *vol. 10*, no. 11, pp. 1726, **2017**.
2. Sherif. O, Zain Elabideen, A. A. Helal, and I. F. El-Arabawy, "Low Voltage Ride Through Capability Techniques for DFIG-Based Wind Turbines," *International Journal of Electrical, Computer, Energetic, Electronic and Communication Engineering*, *vol. 10*, no 7 pp. 910-918, **2016**.
3. M. K. Döşoğlu, "Enhancement of Dynamic Modeling for LVRT Capability in DFIG-Based Wind Turbines," *Iranian Journal of Science and Technology, Transactions of Electrical Engineering*, *vol. 44*, no. 4, pp. 1345–1356, **2020.**

4. X. Zhang, X. Cao, W. Wang, and C. Yun, "Fault Ride-Through Study of Wind Turbines," *Journal of Power and Energy Engineering, vol. 01*, no. 05, pp. 25–29, **2013**.
5. Molina Marcelo and Mercado Pedro, "Modelling and Control Design of Pitch-Controlled Variable Speed Wind Turbines," 2011.
6. F. M. Gebru, B. Khan, and H. H. Alhelou, "Analyzing low voltage ride through capability of doubly fed induction generator-based wind turbine," Computers & Electrical Engineering, vol. 86, p. 106727, **2020**
7. X. Wang, H. Zhang, and Q. Zhang, "The Strategy of Doubly-fed Induction Generator Low-Voltage Ride-Through Based an Integrated Protection Circuit," *IOP Conference Series: Materials Science and Engineering*, vol. 486, pp. 012134, **2019**.
8. S. Tohidi and M. Behnam, "A Comprehensive Review of Low Voltage Ride Through of Doubly Fed Induction Wind Generators," *Renewable and Sustainable Energy Reviews*, vol. 57, pp. 412–419, **2016**.
9. C. M. Rahul Charles, V. Vinod, and A. Jacob, "Field Oriented Control of DFIG Based Wind Energy System Using Battery Energy Storage System," *Procedia Technology*, vol. 24, pp. 1203–1210, **2016**.
10. X. Zhang, X. Cao, W. Wang, and C. Yun, "Fault Ride-Through Study of Wind Turbines," *Journal of Power and Energy Engineering*, vol. 01, no. 05, pp. 25–29, **2013**.
11. N. Amutha and B. Kalyan Kumar, "Improving Fault Ride-Through Capability of Wind Generation System Using DVR," *International Journal of Electrical Power & Energy Systems*, vol. 46, pp. 326–333, **2013**.
12. Jackson John Justo, Francis Mwasilu, and JinWoo Jung, "Doubly-Fed Induction Generator-Based Wind Turbines: A Comprehensive Review of Fault Ride-Through Strategies", *Renewable and Sustainable Energy Reviews Elsevier, vol. 45*, pp. 447-467, **2015**.
13. Boyu Qin, Hengyi Li, Xingyue Zhou, Jing Li, and Wansong Liu, "Low-Voltage Ride-Through Techniques in DFIG-Based Wind Turbines: A Review," *Applied Sciences, vol. 10*, p. 2154, **2020**.
14. M. El-Moursi, P. Kaliannan, R.A. Jerin A, and U. Subramaniam, "A Review on Fault Ride Through Solutions for Improving Transient Stability in DFIG Based Wind Turbines, *IET Renewable Power Generation*, *vol.12*, pp. 1786 – 1799, **2018**.
15. S. O. Amrouche, D. Rekioua, and T. Rekioua, "Overview of Energy Storage in Renewable Energy Systems," *3rd International Renewable and Sustainable Energy Conference (IRSEC)*, **2015**.
16. Luis. A. G. Gomez, A. P. Grilo, M. B. C. Salles, and A. J. Sguarezi Filho, "Combined Control of DFIG-Based Wind Turbine and Battery Energy Storage System for Frequency Response in Microgrids," *Energies*, vol. 13, no. 4, p. 894, **2020.**
17. Gonzalo Abad, Jesús L, M. Rodríguez, L. Marroyo, and Grzegorz Iwanski "Doubly Fed Induction Machine: Modeling and Control for Wind Energy Generation Applications", *Wiley-IEEE Press*, 2011.
18. Dehong Xu, F. Blaabjerg, W. Chen and N.Zhu, "Advanced Control of Double Fed Induction Generator for Wind Power System", *John Wiley & Sons Ltd, United Kingdom*, 2018.
19. Haitham Abu-Rub, Mariusz Malinowski, Kamal Al-Haddad, "Power Electronics for Renewable Energy Systems, Transportation and Industrial Applications", *John Wiley & Sons Ltd, United Kingdom*, pp. 9-12, 2014.
20. Ehsan Dadashnialehi, "Modeling and Control of Variable Speed Wind Turbines", *Master's Thesis*, 2012.
21. Amer Obaid Kareem "Performance Analysis of Doubly-Fed Induction Generator (DFIG)- Based Wind Turbine with Sensor and Sensorless Vector Control", *Ph.D. Thesis*, 2016.
22. Ayala. E, Simani. S, Pozo, N. and Muñoz. E "Indirect Speed Control Strategy for Maximum Power Point Tracking of the DFIG Wind Turbine System.," *Revista Técnica Energía*, *Vol. 17*, Issue 2, pp. 92-101, **2021**.